Publications of the Astronomical Society of the Pacific, 129:055001 (14pp), 2017 May doi:10.1088/1538-3873/aa54a7

Solvepol: A Reduction Pipeline for Imaging Polarimetry Data

Edgar A. Ramírez[1,2], Antônio M. Magalhães[1], James W. Davidson Jr.[3], Antonio Pereyra[4], and Marcelo Rubinho[5]
[1] Instituto de Astronomia, Geofísica e Ciências Atmosféricas, Universidade de São Paulo (IAG-USP), SP 05508-900, Brazil; e.ramirez@usp.br, e.ramirez@inaoep.mx
[2] Instituto Nacional de Astrofísica, Optica y Electrónica (INAOE), 72000 Puebla, Mexico
[3] Astronomy Department, University of Virginia, 530 McCormick Road, Charlottesville, VA 22904-4325, USA
[4] Instituto Geofísico del Perú, Área Astronomía, Calle Badajoz 169, Lima, Perú
[5] Instituto de Astronomia, Geofísica e Ciências Atmosféricas, Universidade de São Paulo, SP 05508-900, Brazil
Received 2016 October 24; accepted 2016 December 19; published 2017 March 31

Abstract

We present a newly, fully automated, data pipeline, Solvepol, designed to reduce and analyze polarimetric data. It has been optimized for imaging data from the Instituto de Astronomía, Geofísica e Ciências Atmosféricas (IAG) of the University of São Paulo (USP), calcite Savart prism plate-based IAGPOL polarimeter. Solvepol is also the basis of a reduction pipeline for the wide-field optical polarimeter that will execute SOUTH POL, a survey of the polarized southern sky. Solvepol was written using the Interactive data language (IDL) and is based on the Image Reduction and Analysis Facility (IRAF) task PCCDPACK, developed by our polarimetry group. We present and discuss reduced data from standard stars and other fields and compare these results with those obtained in the IRAF environment. Our analysis shows that Solvepol, in addition to being a fully automated pipeline, produces results consistent with those reduced by PCCDPACK and reported in the literature.

Key words: ISM: general – polarization – techniques: image processing

Online material: color figures

1. Introduction

The observational basis for astrophysics has been generally developed by measuring the radiation flux or brightness of objects, either in broadband or in spectral form, regardless of the polarization state of the light beam. The polarization of the light has encoded information that can be used to investigate many astronomical phenomena in more detail, such the interstellar medium (ISM), the cosmic microwave background, active galactic nuclei, magnetic cataclysmic variables (polars), among others.

In the last few decades, a grater number of polarimetry and spectropolarimetry studies have been done (e.g., Trujillo-Bueno et al. 2002; Adamson et al. 2005; Bastien et al. 2011). However, large area polarimetric surveys are few, even though they provide an increased database for a much better knowledge of the aforementioned areas of the astronomy.

Efforts towards improving this have led to several surveys in the past few years. Near-infrared (NIR) Galactic Plane Infrared Polarization Survey (GPIPS; Clemens et al. 2012), is a notable one. Another example is the Southern Interstellar Polarization survey (Magalhães et al. 2005), aimed at obtaining optical polarization towards selected areas of (mostly) the Galaxy, in and out of the Plane. SOUTH POL (Magalhães et al. 2012), a broadband, all-sky polarimetric survey in the optical is slated to begin in 2017.

Surveys and/or large area programs, by their nature, typically need to have some form of data reduction pipeline. A 2k × 2k charge-coupled device (CCD) on a moderate, meter-sized telescope might provide several hundred polarized stars from a $\sim 10' \times 10'$ field. SOUTH POL and its 9k × 9k CCD will image a ~ 2 degrees^2 field of view, roughly two orders of magnitude larger, producing tens of thousand of stars per field. With tens of fields observed each night on a shared dedicated telescope, the need to go from the raw frames to a catalog containing photometric, polarimetric and astrometric data in an efficient way becomes thus evident.

Over the years we have developed PCCDPACK (Pereyra 2000; Pereyra & Magalhães 2004), an Image Reduction and Analysis Facility (IRAF) package for reducing polarimetric data. PCCDPACK is used at certain astronomy centers in Brazil, Chile, USA and elsewhere. SOUTH POL and its ~ 2 degrees^2 field of view, along with a shared, dedicated robotic telescope, presented a data reduction challenge given the much large data sets. This paper presents Solvepol, a pipeline to address this need. The main advantage of Solvepol over the previous PCCDPACK routines is that the pipeline reduces the data fully automatically without user interaction—the previous reduction package is semiautomatic—, and speeds up the reduction process.

This paper is organized as follows. The description of the data is presented in Section 2. The description of the pipeline is given in Section 3. Results of pilot studies on polarized standard stars, the field HD110984 and the Musca Dark Cloud, are presented in Section 4. A comparison of the photometry

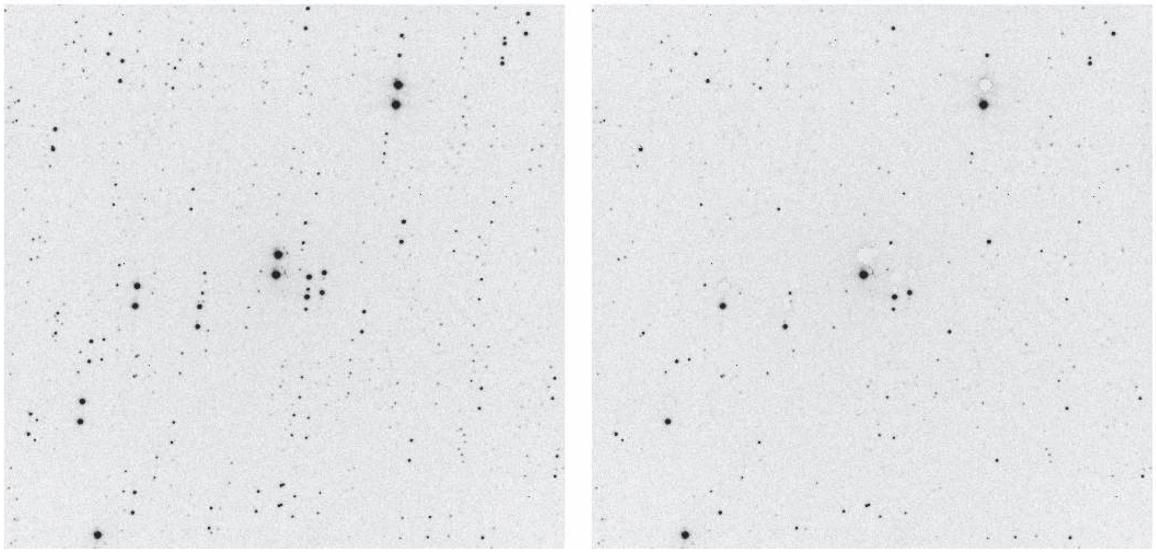

Figure 1. Observations with IAGPOL (Magalhães et al. 1996) mounted on the 0.6 m telescope at OPD, Brazil. Left: field centered on HD110984 ($18 \times 18'$) showing a typical image with the doublet of each star (ordinary and extraordinary) produced by the calcite Savart prism. Right: same field masked out by Solvepol to calculate the astrometry (see Section 3.3).

performed by IDL and IRAF is given in Section 5. The Conclusion presents final considerations.

2. Data Acquisition

The polarimetric data that we have analyzed with this new pipeline was acquired with the IAG-USP optical/NIR imaging polarimeter, IAGPOL (Magalhães et al. 1996), mounted on the 60 cm or 1.60 m telescopes at Observatório do Pico dos Dias (OPD). IAGPOL consists of a half-wave plate that can be rotated in steps of 22°.5, a calcite Savart prism, and the CCD detector. To get the polarimetric properties of an object, a sequence of 4, 8, 12 until 16 maximum observations at adjacent positions of the waveplate are required. For example, a bright object can be observed with a sequence of one exposure per wavelength position, lets say four positions (0°, 22°.5, 45°, and 67°.2); while a dim object, multiple exposures per waveplate position would be more appropriate. The more positions of the waveplate, the more accurate is the polarimetry. The wide area imaging polarimeter for the SOUTH POL survey operates with exactly the same principles, other than the larger size of the optical components.

The calcite Savart plate used in IAGPOL consists of two identical prisms, each cut with their optical axis at 45° to the entrance (and exit) faces, maximizing the beam separation. The two prisms were then cemented together with their optical axis crossed. If a single prism is used, the extraordinary (e) beam will suffer from astigmatism and color dispersion. By cementing the two identical prisms, the ordinary (o) ray coming from the first prism becomes the extraordinary ray for the second prism and vice versa, canceling to a good degree the effects present with a single prism. Also, the o-e and e-o beams will focus essentially on the same plane.

The calcite Savart prism causes each star image to become double on the CCD. Figure 1 shows a typical image obtained when using the IAGPOL showing the star doublets. An advantage of the calcite Savart prism is that, because the ordinary and extraordinary images are perpendicularly polarized to each other, the polarization of the sky around the o-e stellar image is cancelled out (e.g., Magalhães et al. 1996), allowing observations under non-photometric conditions. All the data analyzed was obtained in the *V* filter. During a typical observational campaign, a minimum of one polarized standard star and one non-polarized standard star are observed per night. Several calibrators are thus obtained during each observing run. The unpolarized standard stars are used to obtain the telescope's instrumental polarization, to be subtracted from the measured polarization. The polarized standards are used to transform the instrumental polarization position angle to one in the equatorial system.

3. Description of the Pipeline

Solvepol is written in Interactive Data Language (IDL) and it uses functions and procedures that are found in the IDL Astronomy Library (Landsman et al. 1993) and in the Coyote Graphics Library.[6] It also makes use of Astrometry.net suite (Lang et al. 2010),[7] a very useful software for astrometric purposes that is called by the pipeline.

[6] http://www.idlcoyote.com/

[7] Astrometry.net is a project partially supported by the US National Science Foundation, the US National Aeronautics and Space Administration, and the Canadian National Science and Engineering Research Council. For more information go to http://astrometry.net.

Solvepol corrects the raw images for bias and flats, and calculates the polarization (P), polarization position angle (θ), and the catalog calibrated magnitude (V magnitude, in this case) of the detected stars in the field. The main final product is a catalog in plain text format which also contains the right ascension (R.A.) and declination (decl.) of all stars. The polarization signal-to-noise, P/σ_P, and the ratio F/σ_s, where F is the flux of a star and σ_s is the standard deviation of sky brightness, are initial parameters that can be set by the user and are used to reject weak sources. The complete list of input parameters is described in the Solvepol manual available at http://www.astro.iag.usp.br/~ramirez/pipeline.html.

In addition, we developed two procedures to help analyze the data generated by Solvepol: Merge and Filter.

1. Merge: this merges two catalogs calculating the weighted mean of P, θ (in $Q-U$ space) and V of the stars common to both catalogs. Merge reads the position, R.A. and decl., of stars in two catalogs, and finds stars that match within a box with $0^{\circ}.001$ ($3''.6$) side.
2. Filter: this extracts a subset of a catalog created by Solvepol or Merge by setting lower and upper limits to P, θ, V, and lower limits to P/σ_P and F/σ_s. These limits are set by the user in interactive mode for an ad hoc analysis.

3.1. CCD Frame Calibration

The data reduction procedure that the pipeline applies is based on the standard procedure explained by Massey (1997). Roughly the procedure is as follows:

1. First, the bias frames are median combined. Then, using the IDL SIGMA_FILTER procedure, sigma clipping is applied to remove pixels that deviate by more than 2.5 sigma from the median value of the neighboring 300 by 300 pixels. Finally, the overscan region is fit with a polynomial of order 2 and subtracted to create the master-bias frame.
2. For flat field frames, the overscan region is fit as previously described and is subtracted to each flat field frame. Next, the flat fields are median combined. Then, sigma clipping is applied as before, and the master bias is subtracted to create the master flat frame.
3. Each source image is reduced by first fitting a polynomial of second order to the overscan region, and subtracting this fit from the image. The master-bias is then subtracted and the result is then divided by the master-flat frame normalized to the median of the sky. Finally, the source images are trimmed to remove the overscan region.

If multiple images were observed per position angle of the waveplate, they are median combined after performing the reduction steps outlined above. The pipeline estimates and corrects for any possible shifts in X and Y between images before combining.

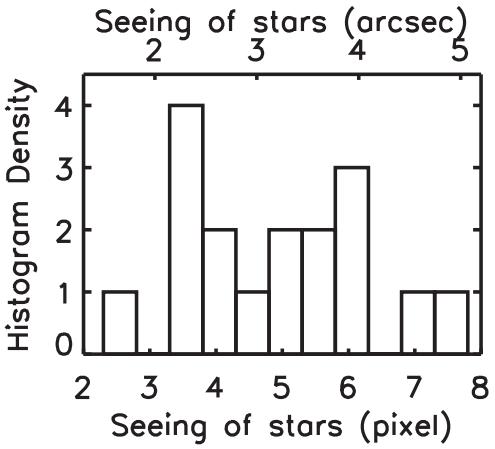

Figure 2. Seeing of standard stars observed with the 60 cm telescope of the OPD in pixel and arcsec units. The seeing ranges from two to eight pixels, thus the 10 pixels concentric apertures to perform the polarimetric measurements is justified.

3.2. Polarization Data Reduction

The pipeline finds all point sources, i.e., stars, and performs photometric measurements which are used to calculate their polarization. Solvepol is not going to find extended sources, and they will be treated as background. Aperture photometry is performed on both ordinary and extraordinary images of each star (F_o and F_e, respectively) with 10 concentric apertures ranging in size from one to 10 pixels in radius. For each aperture an annulus, with fixed inner and outer radii of 10 and 20 pixels respectively, is used to estimate the sky (the default annulus in Solvepol).

These apertures cover up to $\sim 5\times$ the full width at half maximum (FWHM) that the stelar disk may have when observing with the IAGPOL at the OPD. Figure 2 shows the seeing measured in standard stars observed with the 60 cm telescope. The seeing that we get ranges from 2 to 8 pixels ($1''.3$ to $5''.2$), but we know that the seeing of stars distorted due to cirrus is 7 to 8 pixels ($4''.5$ to $5''.2$). Under good observational conditions, we measured a seeing of $\sim$3.5 pixels ($2''.3$). Thus, the 10 concentric apertures will cover all seeing conditions.

The photometry is measured using the same aperture for all waveplate positions, and the aperture size that gives the lowest error in the polarimetry is selected to calculate the final polarimetric properties of a star.

The modulation of the intensity, z_i, where i is one of 16 orientations of the half-wave plate (i.e., $i=1$ to 4, 6, 8, or 16 positions), is

$$\frac{F_{e,i}-F_{o,i}(F_e^T/F_o^T)}{F_{e,i}+F_{o,i}(F_e^T/F_o^T)} = Q\cos(4\,\psi_i)+U\,\sin(4\,\psi_i), \qquad (1)$$

where $F_{o,i}$ and $F_{e,i}$ are the fluxes of the ordinary and extraordinary images at the position i of the waveplate, and F_o^T and F_e^T are the ordinary and extraordinary total flux of a star summed on all the waveplate's positions, respectively (see Magalhães et al. 1984). Q and U refer to the instrumental Stokes parameters of the incoming beam's linear polarization. Equation (1) shows that a set of four waveplate positions (e.g., $i = 1$ through 4) measures Q, U, $-Q$, and $-U$. A linear polarization measurement can then be obtained by doing exposures through 4, 8, 12, or 16 positions of the waveplate, although this cycle can be repeated as needed. The polarimetric properties are estimated following the formulation of Magalhães et al. (1984), which consists in solving for U and Q the expression applying the method of the least squares.

The solution for the stokes parameters Q and U for each source are

$$Q = \frac{2}{\mu}\sum_{i}^{\mu} z_i \cos(4\psi_i) \tag{2}$$

$$U = \frac{2}{\mu}\sum_{i}^{\mu} z_i \sin(4\psi_i), \tag{3}$$

where μ is the number of positions of the half-wave plate and $\psi_i = [i - 1] * 22.^{\circ}5$ (=0°, 22.°5, 45°, 67.°5, etc.). This yields the percent linear polarization, P, and the polarization angle, θ, measured from north to east after the zero-angle is calibrated using polarized standard stars:

$$P = \sqrt{Q^2 + U^2} \tag{4}$$

$$\theta = \frac{1}{2}\tan^{-1}\frac{U}{Q}. \tag{5}$$

The uncertainties of the polarimetric properties are in essence the residual of the actual measurements at each waveplate position angle with respect to the theoretical nonlinear curve of the modulation. Assuming that $\sigma_Q = \sigma_U = \sigma_P$, the error may be calculated as (see Magalhães et al. 1984; Naghizadeh-Khouei & Clarke 1993)

$$\sigma_P = \frac{1}{\sqrt{\mu - 2}}\sqrt{\frac{2}{\mu}\sum_{i}^{\mu} z_i^2 - Q^2 - U^2} \tag{6}$$

$$\sigma_\theta = 28.^{\circ}65\frac{\sigma_P}{P}. \tag{7}$$

The reduced Chi square (χ^2) of the fitted modulation is calculated, and for this work, those stars with $\chi^2 > 6.0$ are rejected. This limit was set by empirical grounds. Figure 3 shows the χ^2 of the stars of the Musca field analyzed in this work (in Section 4). As can be seen, a $\chi^2 = 6.0$ separates reasonably good those stars belonging to the Musca cloud and those showing unexpected high polarization. Therefore, a $\chi^2 \leqslant 6.0$ would include a reasonable sample with real polarization. This test was applied in other fields with same result. However, a different cutoff for χ^2 can be selected by the user of Solvepol either interactively or a priori before running the code.

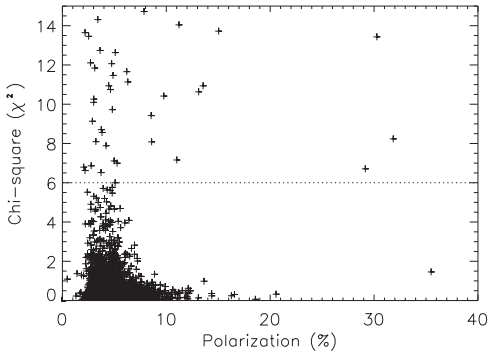

Figure 3. Chi square of the modulation fit vs. Polarization of the stars in Musca fields analyzed in this work. $\chi^2 > 6$ is a reasonable limit to reject stars with bad modulation fit and therefore spurious polarization. The selection is $F/\sigma_s \geqslant 5.0$ and $P/\sigma_P \geqslant 5.0$. Notice that there is a spurious star with $\chi^2 \approx 1$ and $P \approx 35$ that the user should distinguish.

Solvepol doesn't correct for Ricean bias affecting values with $P/\sigma_P \leqslant 3.0$ (Clarke & Stewart 1986). The users of Solvepol must be aware of this and correct their results. The results presented in this work were obtained with $P/\sigma_P \geqslant 5.0$ and 10.0, when indicated; therefore, they are not affected by Ricean bias—only values with $P/\sigma_P \leqslant 3.0$ are affected.

3.3. Astrometry Calibration

Solvepol uses the Astrometry.net software (Lang et al. 2010) to calibrate the astrometry of the image being analyzed to get the accurate celestial coordinates of the stars. The pipeline masks out one of the components of the doublet (always the most right component) of each star emerging from the calcite Savart prism on the first waveplate position's image, to get a "normal" image of the sky. Figure 1 shows the original image from the first waveplate position (left), and after applying the mask (right). For this case the right-up component of each star have been masked. The masked regions are replaced with the mode sky value of the image. The size of the mask is equal to the aperture that gives the lowest uncertainty in P. This "normal" image is processed by the Astrometry.net software.[8]

The Astrometry.net software finds, in the masked image, the relative positions of nearby groupings of three or four stars on the field, and finds their corresponding triples or quadruplets in the 2MASS and Tycho-2 catalogs. Each grouping generates a candidate matching sky, and Astrometry.net finds the true matching view. After an alignment of the image and the

[8] Alternatively, in the case that the astronomy.net software is not installed in the running computer, the "normal" image or a list produced by Solvepol of positions of the detected stars sorted by brightness can be used directly in the Web version of Astrometry.net.

catalog, Astrometry.net calculates the astrometric solution that the pipeline includes in the masked image header. This image/header information is then used to translate from pixels to R.A. and decl. of the detected sources.

The mean accuracy in the position that we calculated by comparing the position of standard stars (see Section 4.1) with that of the literature is $\pm 0\farcs44$. This accuracy allows to search the stars in the Guide Star Catalog, version 2.3 (GSC v2.3. Lasker et al. 2008) to perform the magnitude calibration.

3.4. Photometry and Magnitude Calibration

New photometric measurements are applied to both the ordinary and extraordinary images within an aperture with diameter two times the mean FWHM and the default annulus in Solvepol to estimate the sky background of 10 pixel radius and 10 pixels width. The mean FWHM is estimated of at most 30 of the brightest stars in the field, in the first waveplate position's image. If the FWHM is greater than 10 pixels, an aperture of 10 pixels in radius is used for the photometry. We define the measured flux, F_m, as the sum of the ordinary and extraordinary fluxes. For our observations taken in the V-band, the pipeline obtains the visual magnitude

$$V = m_z - 2.5\log(F_m), \tag{8}$$

where m_z is the zero point magnitude calibrated with the GSC v2.3 (Lasker et al. 2008). This catalog goes down to 18th magnitude.[9] We define m_z as the mean of the absolute difference (to avoid that the sum is zero) between our measured magnitude, $m_{\mathrm{m},i}$, and the optical magnitude reported in the GSC v2.3, $m_{\mathrm{c},i}$, for at most the 25 brightest stars in the field, i.e., $m_z = \frac{1}{k}\sum_{i=1}^{k}|m_{\mathrm{m},i} - m_{\mathrm{c},i}|$, where k is at most 25. If there are no stars with measured magnitude in the catalog GSC v2.3, m_z is set to 0 (no calibration).

4. Results

We conducted pilot studies to test our new pipeline Solvepol. These include the analysis of 10 standard stars (essential for calibration), the field centered on HD110984 (a well-studied field in our group), and the already published 1997 observational campaign on Musca (Pereyra & Magalhães 2004, hereafter PM04). We fixed $F/\sigma_s \geqslant 5.0$ for this present work—a limit for a confident source detection.

4.1. Standard Stars

The analysis of polarized standard stars is essential to check the veracity of our results. For the 10 standard stars shown in Table 1, we preset polarization and magnitude results using Solvepol and compare these with reported values from the literature. The standard stars were observed during different observational campaigns, most of them in the 1997 Musca's campaign (PM04).

Although the standard stars are used to get the zero-angle calibration of the observations, the disposition of the telescope relative to the sky or to different positions of the waveplate inside the polarimeter is not the same between observing campaigns. Hereby, the angle θ is meaningless to compare between stars observed in different campaigns, and it is not tabulated in Table 1. The position of HD100623, HD147084, and HD154445 could not be solved because less than three stars fall in their field—at least three stars are needed to solve the astrometry—therefore, its R.A. and decl. are not tabulated for its comparison with the literature.

Figure 4, shows plots comparing P and V of the standard stars calculated with Solvepol and from the literature. These results are consistent to well within 2σ. The P that deviate by more corresponds to HD147084: our P is lower than the reported in Turnshek et al. (1990) by a factor of 0.9. Because we do not see in Figure 4 a systematic displacement from the line representing the equality, the scatter can be attributed to climatological differences along the observation (clouds, cirrus, etc.).

4.2. HD110984 and its Field

We analyzed the field around HD110984. Figure 5 shows the polarization maps of the field centered on HD110984 solved by Solvepol and by PCCDPACK. The polarization (length of the lines) and position angle (measured from north to east) are indicated. Both maps will lead to the same conclusion about the distribution of the polarization on the field of HD110984. However, there are some discrepancies. Around R.A. 191.85 and decl. −61.22, PCCDPACK solves three stars, while Solvepol solves one star only, which is the brightest star of the group of three stars. Moreover, in the center of the image, corresponding to the standard star HD110984, Solvepol solves precisely for HD110984, while PCCDPACK solves three sources where clearly there is no stars but the spikes of HD110984. This examples indicate that Solvepol is producing reliable results.

Figure 6 shows the distributions of P, θ and V for the HD110984 field measured with Solvepol and the PCCDPACK routines for comparison. We fixed $F/\sigma_s \geqslant 5.0$ and $P/\sigma_P \geqslant 5.0$ for this analysis. The distributions of P, θ and V produced by both routines are quite similar. In particular, the distributions of P and θ indicate that both routines lead to the same conclusion about the polarimetric properties on the field of HD110984. Therefore, both routines give polarimetric properties that will lead to the same conclusions when analyzing the same field.

In Figure 7, we compare P, uncertainty in the polarization (σ_P), θ and V using Solvepol versus those using the PCCDPACK routines. For the same stars found by Solvepol and the PCCDPACK routines, it can be seen that both routines produce

[9] The pipeline code can be modified to calibrate with any catalog available online in the VizieR database over the Web.

Table 1
Standard Stars Analyzed

Star	R.A. J2000	decl. J2000	V (mag)	P (%)	Obs. Date	References
HD80558	09 18 42.44	−51 33 37.69	5.29 ± 0.20	3.25 ± 0.06	1997-04-09	...
	09 18 42.36	−51 33 38.34	5.94 ± 0.01	3.11 ± 0.01	...	a
HD84810	—	—	—	1.67 ± 0.07	1997-04-09	...
	09 45 14.81	−62 30 28.44	3.69 ± 0.03	1.58 ± 0.01	...	a
HD100623	—	—	—	0.04 ± 0.06	1997-04-10	...
	11 34 29.49	−32 49 52.81	6.05 ± 0.01	0.02	...	b
HD110984	12 46 44.84	−61 11 11.91	9.19 ± 0.18	5.64 ± 0.05	2001-03-02	...
	12 46 44.84	−61 11 11.47	8.49 ± 0.16	5.79 ± 0.04	1997-04-12	...
	12 46 44.82	−61 11 11.47	8.55 ± 0.16	5.86 ± 0.03	1997-04-13	...
	12 46 44.84	−61 11 11.58	9.04 ± 0.02	5.70 ± 0.01	...	c
HD111613	12 51 18.05	−60 19 47.79	5.47 ± 0.17	3.20 ± 0.04	1997-04-09	...
	12 51 17.98	−60 19 47.24	5.77 ± 0.01	3.06 ± 0.01	...	a
HD126593	14 28 50.87	−60 32 24.94	8.60 ± 0.29	4.94 ± 0.06	2001-03-02	...
	14 28 50.87	−60 32 25.12	8.70 ± 0.01	5.02 ± 0.01	...	c
HD147084	—	—	—	3.79 ± 0.35	1997-04-10	...
	16 20 38.18	−24 10 09.55	4.66 ± 0.01	4.17 ± 0.01	...	c
HD154445	—	—	—	3.79 ± 0.05	1997-04-10	...
	17 05 32.26	−00 53 31.44	5.65 ± 0.01	3.80 ± 0.08	...	c
HD155197	17 10 15.74	−04 50 03.62	9.60 ± 0.08	4.54 ± 0.09	1997-04-12	...
	17 10 15.75	−04 50 03.67	9.57 ± 0.03	4.63 ± 0.02	...	c
HD298383	09 22 29.77	−52 28 57.65	10.78 ± 0.72	5.17 ± 0.06	2001-03-01	...
	09 22 29.77	−52 28 57.36	10.74 ± 0.37	5.43 ± 0.04	1997-04-13	...
	09 22 29.76	−52 28 57.25	10.78 ± 0.34	5.38 ± 0.06	1997-04-12	...
	09 22 29.77	−52 28 57.25	9.75 ± 0.03	5.23 ± 0.01	...	c

Note. Our measurements and those from the literature (last line for each star) are shown. R.A., decl. and V are from the GSC v2.3 catalog (Lasker et al. 2008); P is from: (a) Bastien et al. (1988), (b) Serkowski et al. (1975) (the error is not provided in this reference) and (c) Turnshek et al. (1990). "—" indicates that the position could not be obtained by the pipeline because of the lack of reference stars on the filed (see Section 4.1 for details), and then the magnitude could not be calibrated by Solvepol.

the same results with each other to within 3σ. Clearly the V-error bar given by PCCDPACK is underestimated because it is unexpectedly lower than the mean error reported in the catalog GSC v2.3 for this field, which is ±0.43. Solvepol, on the other hand, takes the mean error of the magnitude reported in the GSC v2.3 catalog as a lower limit of its V-error, i.e., if Solvepol measures an V-error lower than the mean V-error of the magnitudes reported in the GSC v2.3, Solvepol takes the mean V-error of the magnitude of the catalog as the error. About the mean error in θ in Figure 7, the mean error in theta is $\pm 4\overset{\circ}{.}73$ and $\pm 3\overset{\circ}{.}06$ for Solvepol and PCCDPACK, respectively. A difference as low as $1\overset{\circ}{.}67$ indicates consistency in θ.

In Figure 8 we compare the number of sources detected by Solvepol and PCCDPACK. The number of sources detected by Solvepol tends to be higher than the number of sources detected by the PCCDPACK routines for low values of P/σ_P (with $F/\sigma_s \geqslant 5.0$). However, the number of sources detected by both routines converge towards greater values of P/σ_P. For instance, for $P/\sigma_P = 3.0$, the number of stars detected by Solvepol is 154, and the number of sources detect by the PCCDPACK routines is 134—a difference of 20 detected stars —, while for $P/\sigma_P = 5.0$ (usual ratio for a confident measurement) the difference is just 6 stars (101 and 95 detection by Solvepol and the PCCDPACK routines, respectively). Therefore, our new pipeline seems to be producing more complete catalogs.

4.3. Musca Dark Cloud Data

A comparison of our results with those reported in PM04 of the well studied field of the Musca Dark Cloud is presented in this section. We analyze all the fields observed in the 1997 campaign. The observational details are described in PM04. The source detection limits used in Solvepol were set to $F/\sigma_F \geqslant 5.0$ and $P/\sigma_P \geqslant 5.0$, same limits adopted by PM04, but using the PCCDPACK routines.

In Figure 9 the P, σ_P, θ, and V calculated by Solvepol, and those from the catalog of PM04 are presented. As can be seen, P, σ_P, θ and V are all consistent with each other, with some degree of scattering within 3σ. The catalogs produced by Solvepol were processed with MERGE, therefore, there are no repeated stars from the overlapping field regions and the weighted mean of P, θ and V of those overlapped stars were calculated (see Section 3). On the other hand, the catalog

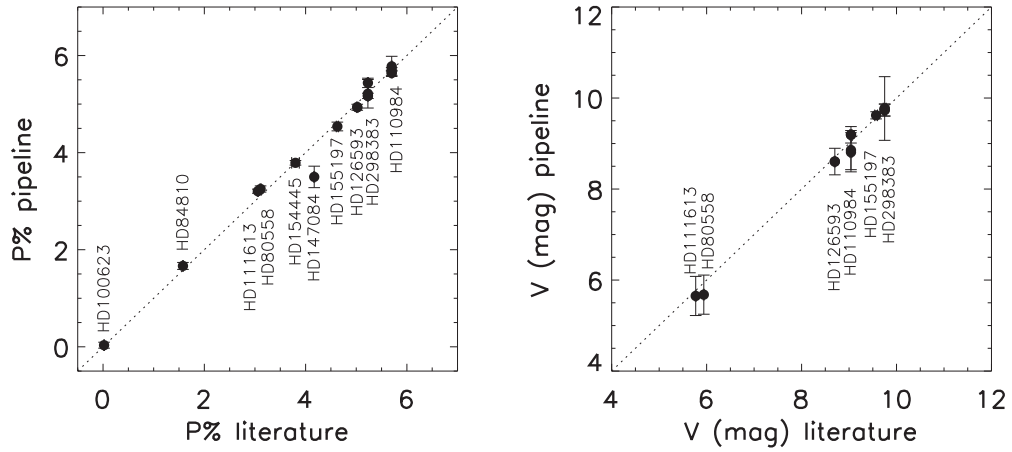

Figure 4. Left: polarization of the standard stars reduced with Solvepol vs. the polarization in the literature (see Table 1). Right: V magnitudes reduced by Solvepol vs. the V magnitude from the GSC v2.3 (Lasker et al. 2008). Dashed line represents the equality. The plotted error bars are 1σ.

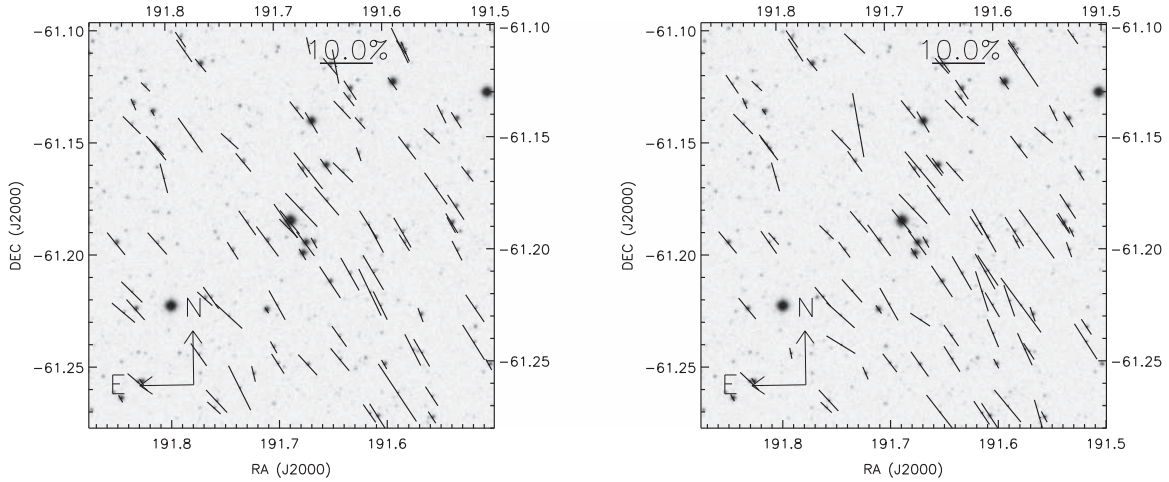

Figure 5. Left: polarization map of the field centered on the standard star HD110984 reduced with the PCCDPACK routines. Right: same field reduced with Solvepol. $F/\sigma_s \geqslant 5.0$ and $P/\sigma_P \geqslant 5.0$.

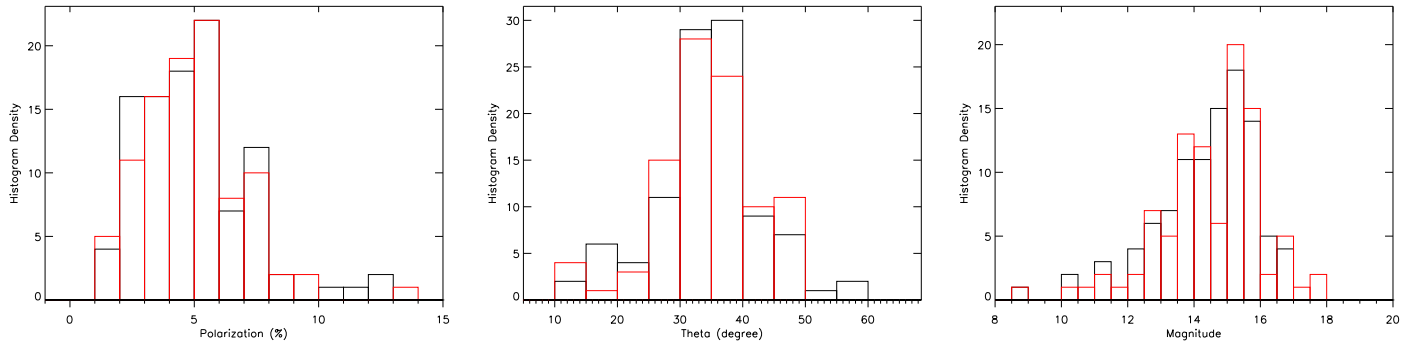

Figure 6. Distributions of P, θ, and V measured by Solvepol (black) and the PCCDPACK routines (red) of the field centered on HD110984. These distributions correspond to $F/\sigma_s \geqslant 5.0$ and $P/\sigma_P \geqslant 5.0$.
(A color version of this figure is available in the online journal.)

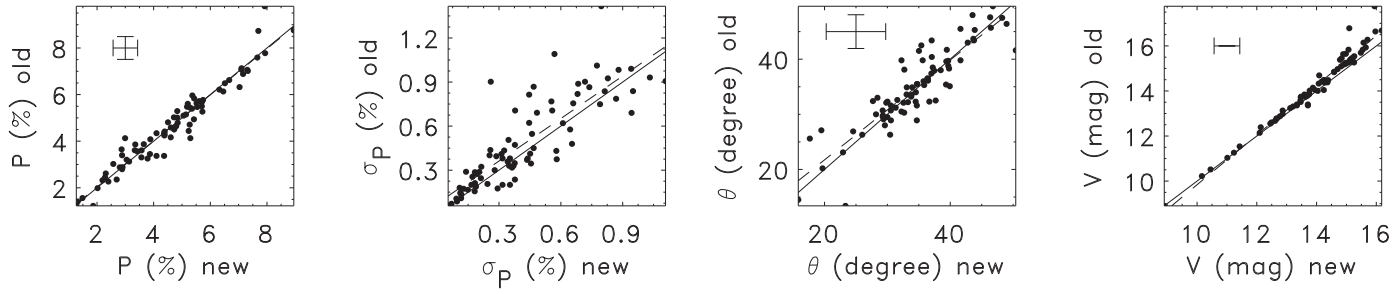

Figure 7. From left to right: P, σ_P, θ, and V measured with Solvepol (new) and those measured by the previous PCCDPACK routines (old) on HD110984's field. Solid line represents the equality; dashed line is a linear fit for comparison. The mean 1σ error bar is indicated.

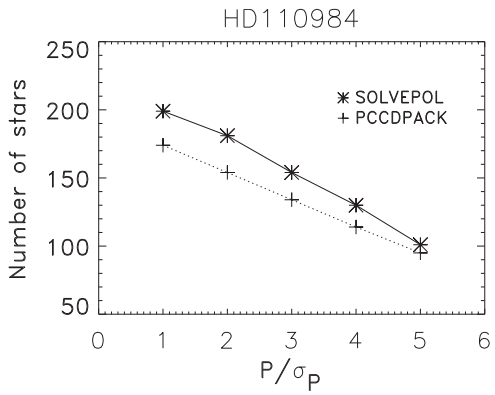

Figure 8. Number of detected stars of the field of HD110984 vs. P/σ_P measured by Solvepol (asterisk signs) and by PCCDPACK (plus signs). F/σ_s is fixed to $\geqslant$5.0. Dotted and solid lines are simply joining the points. Notice that Solvepol gives catalogs with more stars than PCCDPACK, and the number of sources converge towards greater values of P/σ_P. For instance for $P/\sigma_P \geqslant 5.0$ the difference in number of detected stars is only 6.

(reported in VizieR) of PM04 includes two entries for stars in overlapping regions, increasing the total number of results. The uncertainty in V is not reported by PM04, and thus we cannot compare our uncertainties against theirs.

While the error bars in P calculated by Solvepol and PCCDPACK indicated in Figure 9 are consistent, the error bar of θ calculated by Solvepol is slightly bigger than the error bar in θ calculated by PCCDPACK. The mean error in θ is $\pm$4.23 and $\pm$2.66 for Solvepol and PCCDPACK, respectively. This gives a difference of only 1°.57, which indicates that Solvepol and PCCDPACK are in close agreement.

The distributions of P, θ, and V for Musca are shown in Figure 10. The sample reduced with Solvepol seems to be complete in magnitude up to 17 mag. This is 1.5 magnitudes deeper than the 15.5 mag reported in PM04 using PCCDPACK. However, a systematic shift of the estimated magnitudes is clearly seen. To know which magnitudes are offset, we compare both magnitudes with the magnitudes of the GSC v2.3, show in Figure 11. As it can be seen, the magnitudes estimated by Solvepol are closer to the equality line with the magnitude of the GSC v2.3 than those estimated by PCCDPACK: the Solvepol magnitudes fall very close to the equality line, while the magnitudes from PCCDPACK is offset bellow the equality line. Therefore, the magnitude calibration performed by Solvepol is more accurate with the GSC v2.3.

Table 2 shows the field numbers (we have adopted the same notation used in Pereyra & Magalhães 2004), its central position calculated by our pipeline, the number of detected stars, and the weighted mean (as derived in PM04) of P, θ and V with their respective uncertainties calculated by Solvepol, and those from PM04 for comparison. We adopted the same limit of $P/\sigma_P \geqslant 10.0$ adopted by PM04, their table 5, for a direct comparison.

The total number of stars with $P/\sigma_P \geqslant 10.0$ is 857, slightly higher than the 846 sources reported by PM04. About individual fields, the greatest difference in the number of detected stars is only 9 (Solvepol found more) which correspond to field number 24 (see Table 2). However, as it can be seen in Figure 12 (top left plot), that compares the number of sources versus P/σ_P (F/σ_F fix to 5.0) detected by Solvepol and the PCCDPACK routines, the number of sources detected by both routines tend to converge for high values of P/σ_P.

Overall, mean values of P, θ, and V, tabulated in Table 2, and plotted in Figure 12 for an easier inspection, are consistent with the mean values of P, θ, and V reported by PM04 their Table 5, reproduced here in Table 2.

Figure 13 shows the polarization maps on the Musca region of the fields analyzed in this work and tabulated in Table 2 calculated by Solvepol. Each vector represents one object. Again, our polarization maps and those reported by PM04 are in agreement.

It is important to highlight that an important difference between Solvepol and PCCDPACK is that Solvepol is completely automatic, a pipeline without human intervention.

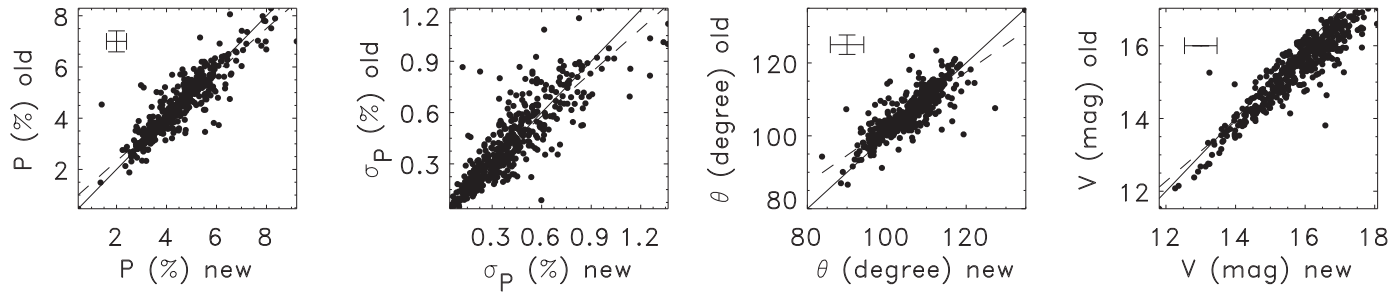

Figure 9. From left to right: P, σ_P, θ, and V measured with Solvepol (new) and those reported in VizieR obtained by PM04 using the PCCDPACK routines (old). $F/\sigma_s \geqslant 5.0$ and $P/\sigma_P \geqslant 5.0$. The solid line represents the equality; the dashed line is a linear fit for comparison. The mean 1σ error bar is indicated. There is no magnitude error bars reported in PM04.

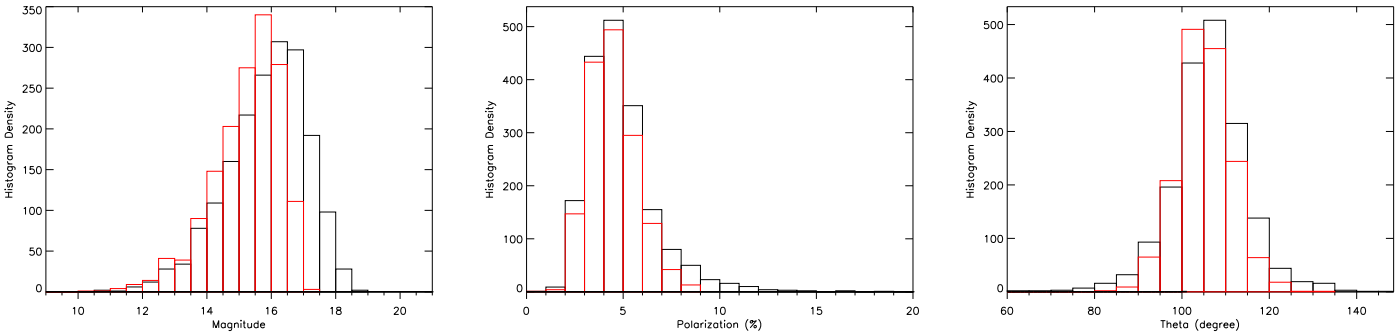

Figure 10. Distributions of P, θ, and V of Musca measured by Solvepol (black) and by the PCCDPACK (red). The selection is $F/\sigma \geqslant 5.0$ and $P/\sigma_P \geqslant 5.0$. (A color version of this figure is available in the online journal.)

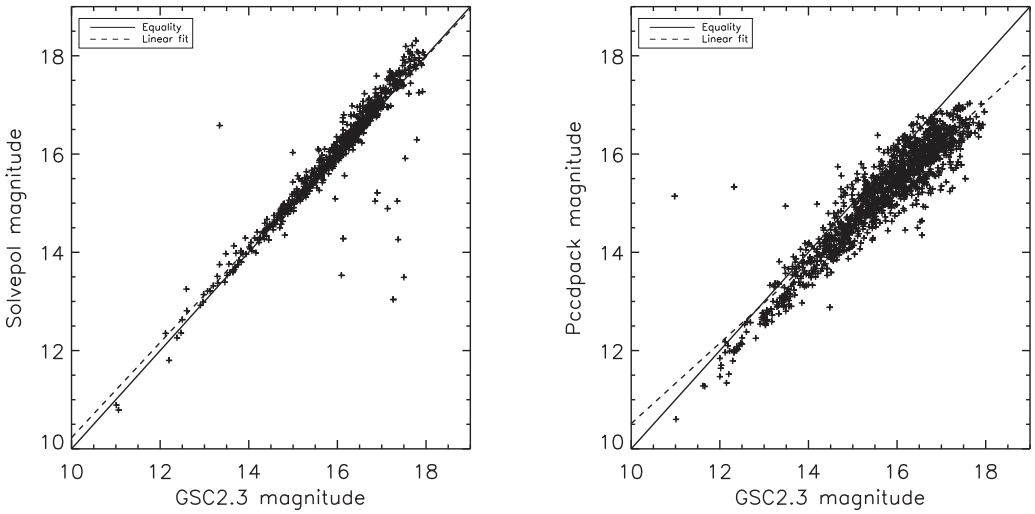

Figure 11. Magnitudes measured by Solvepol (left) and by the PCCDPACK (right) vs. the magnitude reported in the GSC v2.3. The solid line represents the equality; the dashed line is a linear fit for comparison.

The results of PCCDPACK, on the other hand, have been cleaned of stars with unexpected polarimetric values by the user. The results of Solvepol compared in this work have not been post-processed in such a way. Therefore, the raw output of Solvepol is in reasonable agreement with the post-cleaning output of PCCDPACK.

Table 2
Fields of Musca Reduced by Solvepol Using the Values $P/\sigma_P \geqslant 10.0$ and $F/\sigma \geqslant 5.0$

Field	R.A. J2000	decl. J2000	N	mean P (%)	mean θ (°)	mean V (mag)
		Central Region				
03	12 35 05.73	−71 00 30.80	60	3.16 ± 0.02	101.455 ± 1.84	15.46 ± 1.22
05	12 30 06.91	−71 00 35.20	48	3.82 ± 0.02	105.507 ± 1.58	15.50 ± 1.06
08	12 27 36.99	−71 08 40.13	46	3.45 ± 0.03	107.602 ± 2.09	14.94 ± 0.92
11	12 30 10.15	−71 24 38.34	35	3.83 ± 0.03	104.835 ± 1.63	15.41 ± 1.24
13	12 25 13.27	−71 24 40.64	64	5.09 ± 0.02	111.129 ± 1.62	15.47 ± 1.08
14	12 27 43.58	−71 32 35.64	33	2.56 ± 0.03	105.917 ± 1.74	15.63 ± 1.15
16	12 27 50.15	−71 41 00.17	61	4.68 ± 0.03	100.026 ± 1.63	15.73 ± 1.00
20	12 25 12.13	−72 00 56.48	67	4.39 ± 0.02	107.791 ± 1.71	15.29 ± 1.11
22	12 25 18.97	−72 09 19.19	63	4.05 ± 0.02	109.961 ± 1.73	14.92 ± 1.16
24	12 19 58.77	−72 09 33.49	87	4.73 ± 0.02	105.628 ± 1.63	14.91 ± 1.18
26	12 20 06.32	−72 17 26.06	75	5.08 ± 0.02	104.501 ± 1.60	14.86 ± 1.08
27	12 22 33.51	−72 25 16.68	40	4.85 ± 0.03	116.587 ± 1.62	14.87 ± 0.98
29	12 19 57.42	−72 33 32.76	53	4.44 ± 0.02	102.888 ± 1.64	15.10 ± 1.39
30	12 18 02.47	−72 33 39.58	71	3.24 ± 0.02	109.563 ± 1.67	14.41 ± 1.12
34	12 37 56.59	−70 41 10.27	54	2.74 ± 0.02	106.526 ± 1.69	14.42 ± 1.20
03	12 35 27.35	−71 00 31.29	55	3.15 ± 0.02	102.31 ± 1.79	15.45 ± 1.00
05	12 30 28.02	−71 00 34.25	54	3.80 ± 0.02	106.17 ± 1.62	15.47 ± 1.01
08	12 27 58.53	−71 08 35.56	48	3.52 ± 0.03	107.38 ± 1.97	15.50 ± 1.06
11	12 30 28.59	−71 24 34.25	34	3.88 ± 0.03	105.95 ± 1.55	15.34 ± 1.11
13	12 25 29.15	−71 24 36.75	65	4.93 ± 0.02	111.53 ± 1.53	15.43 ± 0.97
14	12 27 59.05	−71 32 35.56	34	3.15 ± 0.03	106.96 ± 1.67	15.37 ± 1.10
16	12 27 59.23	−71 40 35.56	62	4.67 ± 0.03	102.71 ± 1.70	15.47 ± 0.97
20	12 05 29.89	−72 00 36.75	64	4.56 ± 0.03	105.13 ± 1.71	15.42 ± 0.98
22	12 25 30.06	−72 08 36.75	65	3.92 ± 0.02	107.74 ± 1.76	15.43 ± 0.97
24	12 20 15.82	−72 08 38.87	78	4.70 ± 0.02	102.45 ± 1.57	15.48 ± 1.00
26	12 20 15.95	−72 16 38.87	68	5.03 ± 0.02	101.81 ± 1.60	15.44 ± 1.00
27	12 22 53.25	−72 24 37.87	49	5.17 ± 0.03	113.36 ± 1.65	15.48 ± 1.05
29	12 20 16.23	−72 32 38.87	52	4.51 ± 0.02	99.72 ± 1.70	15.50 ± 1.03
30	12 17 39.05	−72 32 39.74	69	3.25 ± 0.02	107.20 ± 1.64	15.45 ± 1.00
34	12 38 03.74	−70 40 29.55	49	2.67 ± 0.02	104.24 ± 1.74	15.48 ± 1.05

Note. R.A. and decl. are the central position of the field. N is he number of detected sources in each field. Weighted mean of P, θ and V and its standard deviation following the same procedure detailed in PM04. Below, the same fields of musca reported by PM04 and using the same P/σ_P and F/σ limits.

5. Comparison between IDL and IRAF Photometric Routines

An aspect to note is that there are stars in the final catalog by Solvepol, but are not in the final catalog produced by the PCCDPACK routines, and vice versa. This can be seen in Figure 5, which shows the polarization maps of the field of the standard star HD110984 solved by Solvepol and by PCCDPACK. The difference in the final result could be due to differences in the photometry performed by Solvepol and PCCDPACK; Solvepol is written in IDL and PCCDPACK is written in IRAF and FORTRAN.

To explore this possibility, we performed photometry with IDL and IRAF using the same input parameters in the same image. We have used an aperture of six pixels radius (∼2 times FWHM; this aperture size collects ∼95% of the light of a star) and the default annulus of Solvepol (inner radius of 10 pixels and 10 pixels width) to perform sky background subtraction, centered on the same position, X and Y, given by Solvepol (re-centering is turned off). In Figure 14 we present the comparison of the photometry performed by the two routines.

The ratio of the SUM shows a scatter from the equality line of around 1%. The standard deviation (SD) from the mean of the SUM ratio is $SD_{SUM} = 0.001$. This scatter can be attributable to rounding, meaning that the SUM by IDL and IRAF are equal. As can be seen, there is an order of 1% difference in the SKY values up to 5%. The standard deviation for this case is $SD_{SKY} = 0.015$. Both IDL and IRAF take the mode of the sky within the annulus (our used annulus has the same size). For the AREA of the aperture used to perform the photometry, there is a scatter of 1%, attributable to rounding, and the $SD_{AREA} = 0.001$. A difference of order 10% and up to 50% in the FLUX (=SUM − SKY ∗ AREA) ratio is clear. The standard deviation from the mean increases to dimmer sources; the SD_{FLUX} goes from 0.020 to 0.367 (see the gray shadowed areas in the plot of the FLUX ratio in Figure 14). This indicates that there is greater scatter in flux

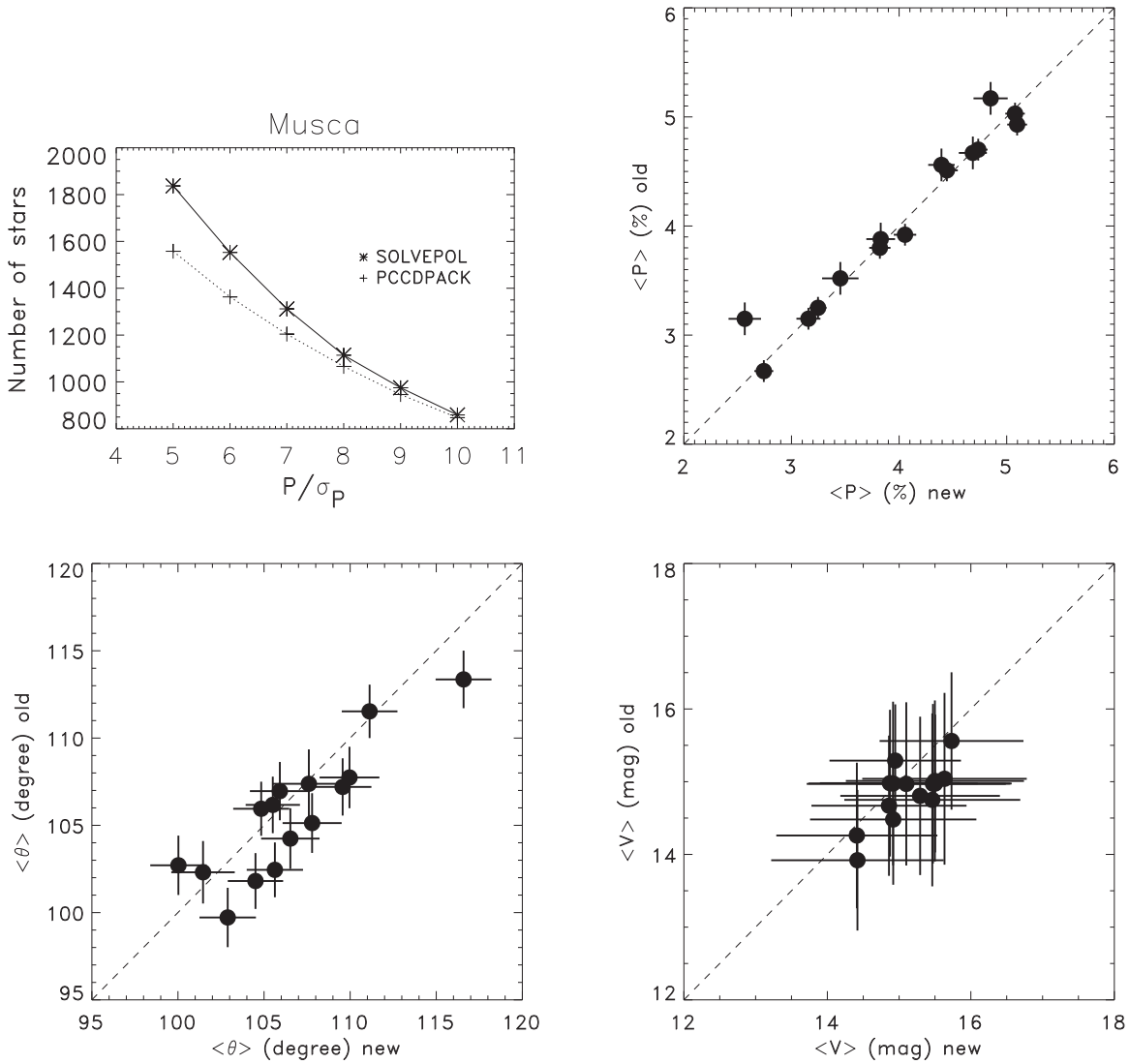

Figure 12. Top left: number of detected stars of Musca vs. P/σ_P measured with Solvepol (asterisk signs) and the number of sources reported in VizieR obtained by PM04 using the PCCDPACK routines (plus signs). F/σ_s is fixed to $\geqslant$5.0. Clearly, the number of sources converge towards greater values of P/σ_P. For the next plots $F/\sigma_s \geqslant 5.0$ and $P/\sigma_P \geqslant 10.0$. Top right: weighted mean values of P measured with Solvepol (new) and weighted mean values of P reported in VizieR obtained by PM04 (old). The errors have been amplified by 5 for an easier inspection. Bottom left: weighted mean values of θ measured with Solvepol (new) and weighted mean values of θ reported in VizieR obtained by PM04 (old). Bottom right: mean values of V measured with Solvepol (new) and mean values of V reported in VizieR obtained by PM04 (old). The error bars are our weighted standard deviation from the mean and those reported by PM04, which we took directly from their table. The data of these plots are also reproduced in Table 2.

for fainter sources (left side of the plot) than for bright sources (right side of the plot).

Although there is 1% scatter in the ratio of the SUMs and AREA, clearly the main source of scatter in the final FLUX ratio is the difference in the SKY values measured by IDL and IRAF, that diverge by up to 5%. Moreover, the faint stars are more affected by the different value of the SKY than the bright stars.

Hence, the photometry performed by IDL and IRAF on the same input image do not always give identical fluxes. The difference in the value of the SKY (5%) gives place to a difference of the FLUX of ∼50% for fainter stars, and less that 10% for bright stars. This difference in FLUX in turns is propagated through all the pipeline and leads to the difference observed in the final catalogs.

As expected, the difference in the value of the FLUX affects the final polarization. In the Figure 15 we compare the ratio of the polarization estimated by Solvepol and PCCDPACK versus optical magnitude. The SD from the mean for stars with

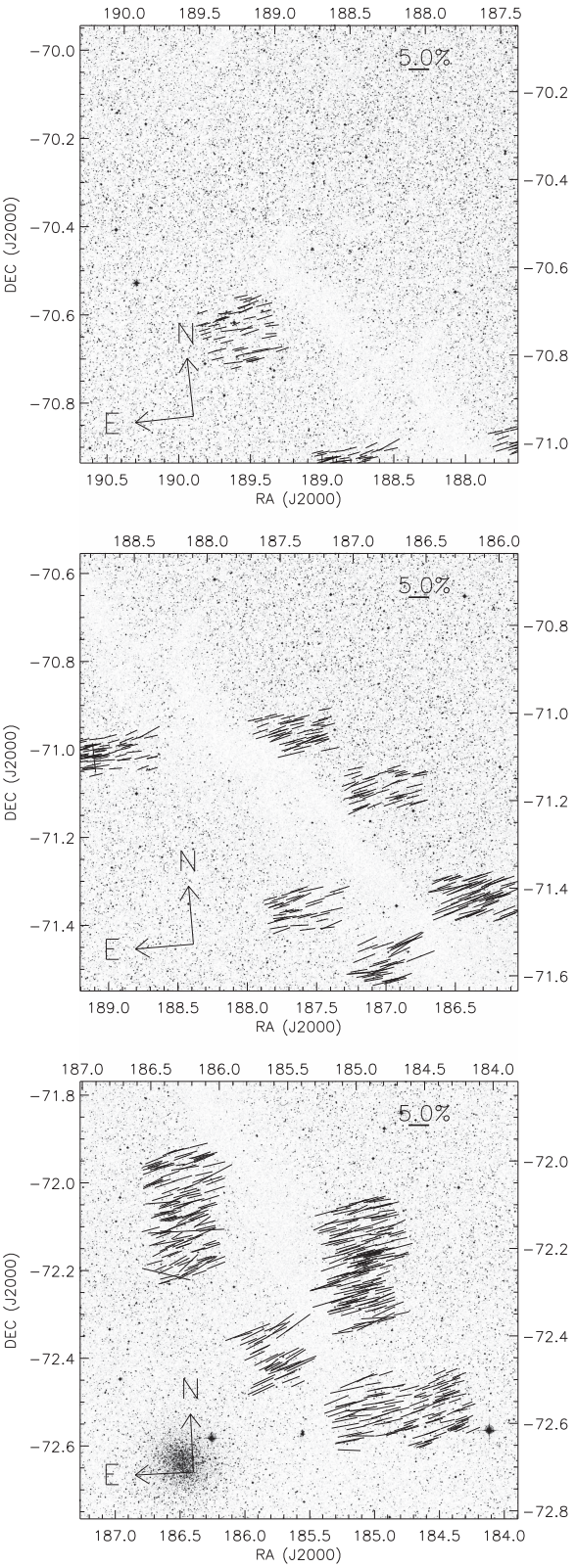

Figure 13. Polarization maps of Musca produced with Solvepol to compare with those in PM04. The selection is $F/\sigma \geqslant 5.0$ and $P/\sigma_P \geqslant 10.0$.

magnitudes dimmer than V 16 mag is 0.442, greater than the SD for brighter stars (see Figure 15). Therefore, the value of the sky affects principally fainter stars ($V \geqslant 13 - 14$ mag). For bright stars the difference is nebligible, and the samples obtained by Solvepol and PCCDPACK are the same.

We found that the different procedures to estimate the sky within the annulus introduces the main scatter. IDL and IRAF estimates the mode of the sky around the photometric apertures in a slightly different way. IDL fits a Gaussian to the array of the sky values to estimate the mode of the background, eliminating outlier pixels from the Gaussian distribution to avoid contamination by stars, and the mode of the sky is obtained after 20 iterations. IRAF estimates the mode of the sky calculating it directly from the sky vector. The different procedures cause the flux, and consequently the final polarization to be not exactly the same, mainly for the fainter stars, and produce the difference in the final catalogs.

6. Conclusions

We have described Solvepol, a new pipeline for reducing imaging polarimetry data obtained with the polarimeter IAGPOL, and that will be used in SOUTH POL.

From the raw images, Solvepol produces a catalog of the observed field with photometric, polarimetric and astrometric information, as well as plots and tables for an inspection and analysis of the results. We have compared results from Solvepol with those from PCCDPACK and found them to be consistent. There is a tendency for Solvepol to produce more complete catalogs due to rounding errors and small differences in the codes.

A clear advantage of Solvepol over PCCDPACK is that it produces a final catalog in hours or minutes, while for a user habituated with PCCDPACK it could take hours or days to produce the final catalog.

As it stands, Solvepol is directly applicable to images obtained with birefringent polarizers, such as the simple calcite plate and the calcite Savart prism. It should not be difficult to adapt it to single-image polarizers, such as dichroic polarizers. Another work in progress is adapting the pipeline to NIR imaging polarimetry. The current version of Solvepol will be made available as a free download at http://www.astro.iag.usp.br/~ramirez/pipeline.html. It is expected that the optical/IR polarimetry community can contribute to its continuous improvement.

E.A.R. acknowledges FAPESP grant (2012/00185-8) and the financial support from the Mexican Council of Science and Technology (CONACyT). A.M.M. acknowledges support for his group's activities at IAG from the agencies FAPESP (grant no. 2010/19694-4), CNPq and CAPES. J.W.D. acknowledges funding from the Brazil-U.S. Physics Ph.D. Student & Post-doc Visitation Program sponsored by the Sociedade Brasileira de

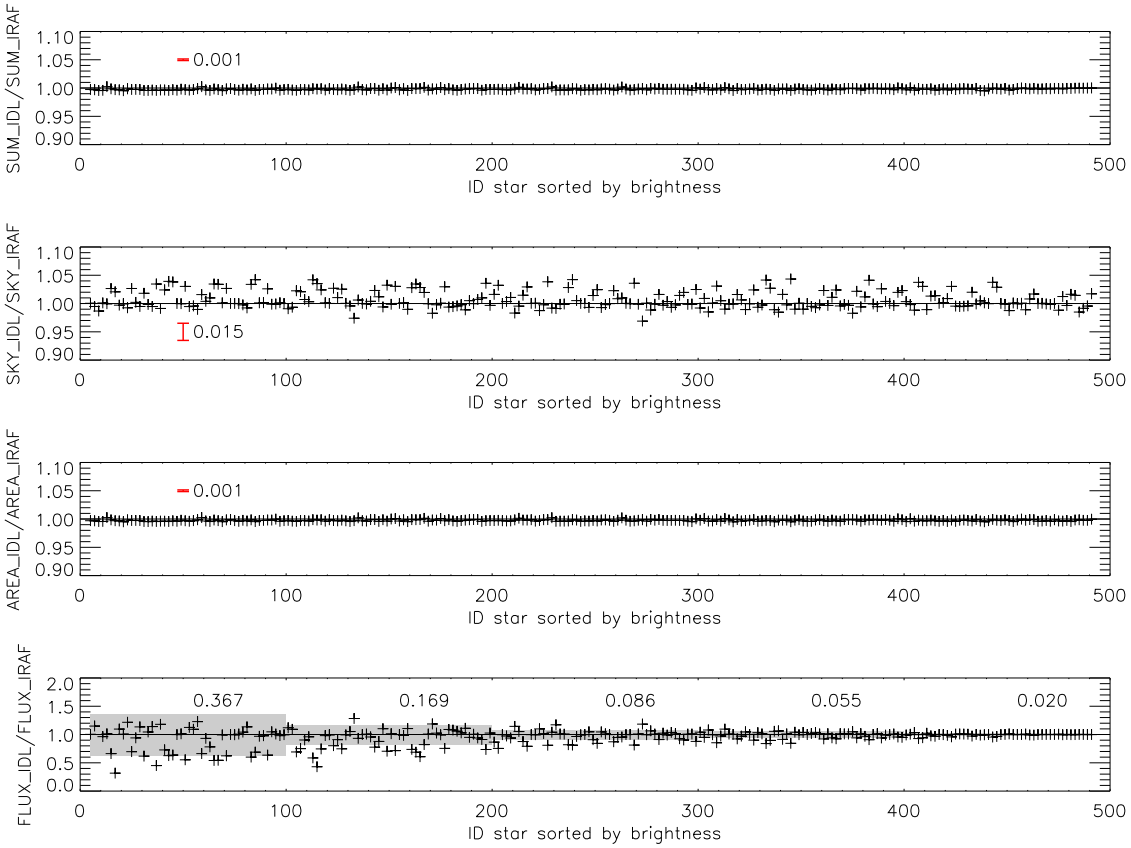

Figure 14. Comparison of the photometry performed with IDL and IRAF vs. an identification number of the stars sorted by brightness (dimmest sources to the left, brightest sources to the right). From top panel to bottom panel: (a) the ratio of the total value in counts within the six pixels radius aperture (SUM); (b) the ratio of the values of the sky within the used annulus (SKY); (c) the ratio of the area of the aperture (AREA); and (d) the ratio of the final fluxes (FLUX). The standard deviation from the mean and its value is indicated for each plot by the red bar. In the case of the FLUX, the standard deviation from the mean were calculated in ranges of ID (indicated by the gray-shaded areas and its value given above each gray area), because the scattering variates with brightness.
(A color version of this figure is available in the online journal.)

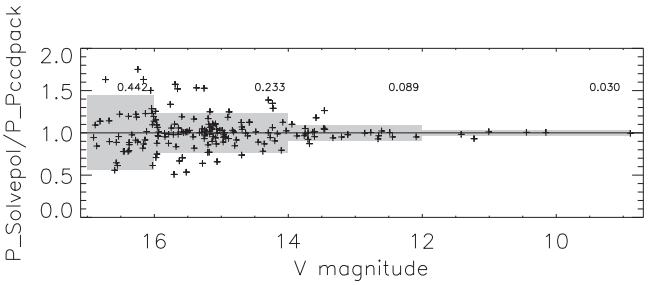

Figure 15. Comparison of the polarimetry calculated with Solvepol and PCCDPACK sorted by magnitude (dimmest sources to the left). The gray-shaded areas are the standard deviation from the mean in ranges of magnitude. The values of the standard deviation for each range are given above each grey area.

Física and the American Physical Society. This research has made use of the VizieR catalog access tool, CDS, Strasbourg, France. The original description of the VizieR service was published in A&AS, 143, 23. The authors thank the first and second anonymous referees for the constructive comments. This research has been partly supported by Mexican CONACyT research grant CB-2011-01-167291.

References

Adamson, A., Aspin, C., Davis, C., & Fujiyoshi, T. (ed.) 2005, in ASP Conf. Ser. 343, Astronomical Polarimetry: Current Status and Future Directions (San Francisco, CA: ASP)
Bastien, P., Manset, N., Clemens, D. P. et al. (ed.) 2011, in ASP Conf. Ser. 449, Astronomical Polarimetry 2008: Science from Small to Large Telescopes (San Francisco, CA: ASP)
Bastien, P., Drissen, L., Menard, F., et al. 1988, AJ, 95, 900
Clarke, D., & Stewart, B. G. 1986, VA, 29, 27
Clemens, D. P., Pinnick, A. F., Pavel, M. D., & Taylor, B. W. 2012, ApJS, 200, 19
Landsman, W. B. 1993, in ASP Conf. Ser. 52, Astronomical Data Analysis Software and Systems II, ed. R. J. Hanisch, R. J. V. Brissenden, & J. Barnes (San Francisco, CA: ASP), 246
Lang, D., Hogg, D. W., Mierle, K., Blanton, M., & Roweis, S. 2010, AJ, 139, 1782
Lasker, B. M., Lattanzi, M. G., McLean, B. J., et al. 2008, AJ, 136, 735
Magalhães, A. M., Benedetti, E., & Roland, E. H. 1984, PASP, 96, 383

Magalhães, A. M., de Oliveira, C. M., Carciofi, A., et al. 2012, in AIP Conf. Ser. 1429, South Pol: Revealing the Polarized Southern Sky, ed. J. L. Hoffman, J. Bjorkman, & B. Whitney (New York: AIP), 244
Magalhães, A. M., Pereyra, A., Melgarejo, R., et al. 2005, in ASP Conf. Ser. 343, Astronomical Polarimetry: Current Status and Future Directions, ed. A. Adamson et al. (San Francisco, CA: ASP), 305
Magalhães, A. M., Rodrigues, C. V., Margoniner, V. E., Pereyra, A., & Heathcote, S. 1996, in ASP Conf. Ser. 97, Polarimetry of the Interstellar Medium, ed. W. G. Roberge & D. C. B. Whittet (San Francisco, CA: ASP), 118
Massey, P. 1997, A User's Guide to CCD Reductions with IRAF, (http://iraf.noao.edu/docs/recommend.html)
Naghizadeh-Khouei, J., & Clarke, D. 1993, A&A, 274, 968
Pereyra, A. 2000, PhD thesis, Depto. de Astronomia, Instituto Astronômico e Geofísico USP, Rua do Matão 1226, Cidade Universitária 05508-900 São Paulo SP, BRAZIL
Pereyra, A., & Magalhães, A. M. 2004, ApJ, 603, 584
Serkowski, K., Mathewson, D. S., & Ford, V. L. 1975, ApJ, 196, 261
Trujillo-Bueno, J., Moreno-Insertis, F., & Sanchez Martinez, F. 2002, Astrophysical Spectropolarimetry (Cambridge: Cambridge Univ. Press)
Turnshek, D. A., Bohlin, R. C., Williamson, R. L., II, et al. 1990, AJ, 99, 1243